R.K. Walter, et al. (2018), Hydrodynamics in a shallow seasonally low-inflow estuary following eelgrass collapse, *Estuarine, Coastal and Shelf Science*, 213, 160-175.

Hydrodynamics in a shallow seasonally low-inflow estuary following eelgrass collapse

Ryan K. Walter[a,*], Edwin J. Rainville[b], Jennifer K. O'Leary[c]

[a] *Physics Department, California Polytechnic State University, San Luis Obispo, CA, USA*
[b] *Mechanical Engineering, California Polytechnic State University, San Luis Obispo, CA, USA*
[c] *California Sea Grant, Department of Biology, California Polytechnic State University, San Luis Obispo, CA, USA*

ARTICLE INFO

Keywords:
Estuarine hydrodynamics
Environmental gradients
Hypersalinity
Ecological regime shift
Exchange processes
Seagrass

ABSTRACT

Hydrodynamics play a critical role in mediating biological and ecological processes and can have major impacts on the distribution of habitat-forming species. Low-inflow estuaries are widespread in arid regions and during the dry season in Mediterranean climates. There is a growing need to evaluate dynamics and exchange processes in these systems and the resultant ecological linkages. We investigate the role that hydrodynamics play in shaping environmental gradients in a short and seasonally low-inflow estuary located along the central California coast. Since 2007, eelgrass meadows in Morro Bay have declined by more than 90%, representing the collapse of the major biogenic habitat. Despite the large-scale decline, eelgrass beds near the mouth of the bay remain resilient, suggesting that conditions in certain areas of the bay might allow or impede eelgrass retention and recovery. Oceanographic moorings were deployed throughout the bay during the summer dry season to assess spatial differences in environmental conditions and hydrodynamics across gradients in eelgrass survival. Relative to the mouth of the bay, the back bay water mass was significantly warmer (hyperthermal), more saline (hypersaline), less oxygenated, and more turbid, with longer flushing times, all of which have been identified as significant stressors on seagrasses. Moreover, there is weak exchange between the mouth and the back bay that effectively decouples the two water masses during most periods. Though the causes of the decline are not clear, gradients in environmental conditions driven by bay hydrodynamics appear to be preventing eelgrass recovery and restoration attempts in the back bay and keeping this region in an alternative state dominated by unvegetated intertidal mudflats. Ecosystems in low-inflow estuaries may be especially prone to ecological regime shifts or collapse and may require precautionary monitoring and management. This system and the dramatic ecological change that it has experienced, demonstrate the critical role that hydrodynamics play in ecosystem health and habitat suitability.

1. Introduction

Coastal ecosystems and estuaries are among the world's most productive ecosystems, but are under increasing threat from climate change, pollution, and development (Short and Wyllie-Echeverria, 1996; Orth et al., 2006; Halpern et al., 2008; Waycott et al., 2009). In these systems, hydrodynamics mediate various ecological and biological processes. Furthermore, the spatial and temporal variations of these hydrodynamic processes and associated changes to the local environment can have major impacts on the distribution of various species, including habitat forming species and the biodiversity they support (cf., Van der Heide et al., 2007; Hansen and Reidenbach, 2012, 2013; Wilson et al., 2013; Carr et al., 2016; Boch et al., 2018; Phelan et al., 2018). With the rapid rise of anthropogenic and climatic stressors and modification to shorelines in marine systems worldwide, an improved understanding of the coupling between hydrodynamics and other key processes in estuarine and coastal environments is needed.

Low-inflow estuaries (LIEs) are common in arid regions, or during the dry season in Mediterranean climates (i.e., seasonal LIEs), but the dynamics of LIEs have received considerably less attention in the literature relative to “classical” estuaries with more persistent freshwater inflow (cf. Largier et al., 1997, 2013; Largier, 2010; Nidzieko and Monismith, 2013). In LIEs, freshwater inputs are inadequate to stratify the estuaries during large portions of the year, and exchange between the estuary and open ocean is controlled by tidal diffusion, as opposed to the classical two-layer estuarine circulation observed in systems with substantial freshwater inputs (Largier et al., 1997; Largier, 2010). In many cases, weak tidal mixing near the head of LIE estuaries can lead to

* Corresponding author.
E-mail address: rkwalter@calpoly.edu (R.K. Walter).

long residence times and the development of various along-estuary (i.e., longitudinal) zones with distinct water mass properties (Largier, 2010; Buck et al., 2014). When the residence times are long relative to the time scales of evaporative surface fluxes, hypersaline basins develop, and depending on the degree of hypersalinity and the prevailing temperature gradients, inverse estuaries can also form (Largier et al., 1997; Nidzieko and Monismith, 2013). As noted by Largier (2010), there is a growing need to not only document and describe the dynamics and exchange processes in small to moderate-sized LIEs, but also to better understand the ecological linkages such as larval retention, species distribution, and habitat suitability (cf. Buck et al., 2014; Morgan et al., 2014; Schettini et al., 2017).

Shallow coastal and estuarine environments are often dominated by seagrass meadows, a critically important biogenic habitat that supports ecosystem function (Waycott et al., 2009). However, seagrasses are sensitive to changing environmental conditions and have been declining worldwide, with the rate of loss increasing substantially over the last century (Orth et al., 2006; Waycott et al., 2009). Loss rates of seagrass meadows are comparable to those reported for tropical rainforests, mangroves, and coral reefs, placing them among the most threatened ecosystems on the planet, despite receiving considerably less attention in the literature and public (Waycott et al., 2009). The rapid declines have been attributed to a variety of different stressors acting on global, regional, and local scales (Orth et al., 2006). These include a variety of physical and biological factors such as increased temperatures, salinity changes, extreme weather events, sedimentation, hypoxia, altered wave and current patterns, wasting disease, eutrophication, and competition with other macroalgae, among others (see Table 1 in Short and Wyllie-Echeverria (1996) and the references therein; Table 1 in Orth et al. (2006)). On a local scale, seagrasses are often influenced by multiple stressors, highlighting the need for a better understanding of how spatiotemporal variations in environmental conditions help shape seagrass populations and influence restoration efforts (cf. Orth et al., 2006).

Accelerated losses of seagrasses can have a profound impact on estuarine systems because they support a diverse range of fish, invertebrates, and resident and migratory birds (Short and Wylie-Echeverria, 1996; Fonseca and Uhrin, 2009; Holsman et al., 2006; Waycott et al., 2009; Shaughnessy et al., 2012). Given their importance and sensitivity to loss, seagrasses are often regarded as biological sentinels, or “coastal canaries” (Orth et al., 2006). Further, seagrasses are ecosystem engineers that strongly modify their physical (and biological) environment and maintain the environment in a state that supports their growth (Van der Heide et al., 2007; Maxwell et al., 2017). When physical conditions change, either abruptly or slowly over time, there is a possibility for ecological regime shifts, where an ecosystem changes it structure and function (Scheffer et al., 2001; Andersen et al., 2009). When an ecosystem enters a new regime, attributes of the changed system can prevent the system from returning to its original state, even after initial conditions are restored (Mayer and Reitkerk, 2004). Since seagrasses are ecosystem engineers, once lost, physical conditions (e.g., turbidity, flow, and light) may change in their absence and make recolonization and restoration attempts difficult through reinforcing feedback loops (Van der Heide et al., 2007; Carr et al., 2016; Maxwell et al., 2017; Moksnes et al., 2018). Thus, positive (self-amplifying) feedback mechanisms in seagrass systems can weaken seagrass resilience when conditions change (Nyström et al., 2012; Maxwell et al., 2017). For example, when seagrass beds were lost in the Dutch Wadden Sea due to a wasting disease, altered hydrodynamics prevented recovery (Van der Heide et al., 2007). Specifically, in the absence of seagrass beds, sediments became destabilized and currents and waves were no longer reduced, resulting in suspended sediment and turbidity levels too high to maintain seagrass growth and thus perpetuating the loss of seagrasses.

LIEs represent a class of estuaries that may be especially prone to changes in environmental conditions that can impact seagrass and the

Table 1
Experimental setup and mooring configuration in 2016.

Mooring Name	Sampling Period (2016)	Mean Water Depth	Text Reference	Measured Parameters	Sampling Period	Instrument Height (mab)	Sensor Type
BM (Bay Mouth)	29 Jun to 4 Aug	7.3 m (8.3 m for ADP)	BM	Velocity	10 min avg (1 s)	First bin at 0.5 mab (0.3 m bins)	Nortek 2.0 MHz ADP
			BM Bottom	Dissolved Oxygen	1 min	1.4	PME MiniDOT
				Temperature	5 s	1.4, 2.6, 3.8, 6.1	Sea Bird 56
				Temperature/Conductivity/Pressure	15 s	2	Sea Bird 37 SMP
				Chlorophyll/Turbidity	15 min (2 min burst avg)	2.9	WET Labs ECO NTU
			BM Top	Temperature/Conductivity/Pressure	15 min (2 min burst avg)	5.6	Sea Bird 37 SIP
				Dissolved Oxygen		5.6	Aanderaa Optode
BC (Bay Center)	29 Jun to 4 Aug (22 Jul to 4 Aug for ADP)	4.8 m (5.3 m for ADP)	BC	Velocity	10 min avg (1 s)	First bin at 0.5 mab (0.3 m bins)	Nortek 2.0 MHz ADP
				Temperature	5 s	0.9	Sea Bird 56
				Temperature/Conductivity/Pressure	2.5 min	1.2	Sea Bird 37 SMP
				Dissolved Oxygen	2.5 min	1.2	Sea Bird 63 Optode
BH (Bay Head)	29 Jun to 4 Aug	2 m*	BH	Temperature	5 s	0.5*	Sea Bird 56
				Dissolved Oxygen	1 min	0.5*	PME MiniDOT
				Chlorophyll/Turbidity	30 min (2 min burst avg)	0.5*	WET Labs ECO NTU

*Estimate based on diver depth gauges and referencing to BC.

associated biodiversity, given the weak exchange and long residence times during low-inflow conditions. Here, we investigate the role that hydrodynamics play in shaping environmental gradients in Morro Bay, a short and relatively understudied LIE located along the central California coast. Since 2007, eelgrass (*Zostera marina*; a temperature seagrass) meadows in this system declined by over 90%, from 139 ha to less than 6 ha, representing the collapse of the major biogenic habitat in this system (MBNEP, 2017). Despite the large-scale decline, eelgrass beds in portions of the bay remain resilient suggesting that environmental conditions and hydrodynamics in certain areas of the bay might allow or impede eelgrass retention and recovery. The goal of this study is to evaluate spatial patterns in hydrodynamics and water quality in relation to eelgrass distribution. This study also describes dynamics in an understudied estuary type (LIE) and elucidates factors that may be impeding eelgrass growth. By evaluating hydrodynamics in an estuary that has experienced sudden and rapid habitat loss, this study provides insight into the role hydrodynamics may play in ecosystem functioning, a link with applications to other estuaries globally.

2. Materials and methods

2.1. Study site

Morro Bay is a shallow estuarine system located along an understudied stretch of the California coast, south of Monterey Bay and north of Point Conception. Morro Bay supports diverse fish, invertebrate, and bird populations; is a major stop along the Pacific Flyway for migratory birds including brant geese (*Branta bernicla nigricans*), which have seen a considerable reduction in wintering populations in Morro Bay following the eelgrass decline (MBNEP, 2017); is a popular tourist destination; and contains aquaculture facilities and a major fishing port for local fisheries. The tidally-forced estuary is characterized by a narrow and progressively shallower channel that runs from the mouth in the north to the back of the bay (i.e., the head) in the south (Fig. 1). The mouth of Morro Bay requires periodic (typically annual) dredging to maintain sufficient depths for commercial fishing and recreational vessels (Fig. 2). The main channel is flanked by large expanses of intertidal flats, particularly in the mid to back portions of the bay, which historically were dominated by large expanses of eelgrass (*Zostera marina*; Fig. 1). Compared to other previously-studied LIEs, Morro Bay is relatively short (~6.5 km long; cf. Largier et al., 1997).

The watershed adjacent to Morro Bay encompasses a drainage area of approximately 190 km^2, with the primary land use being ranchland, brushland, and agricultural, with some residential areas (7% of land use). The watershed drains west primarily through Chorro Creek and Los Osos Creek, with the majority of flow and sediment loading occurring through Chorro Creek (an estimated 86% of the approximately 63,500 metric tons of sediment per year on average; MBNEP, 2015). Similar to other estuaries in Mediterranean climates (Largier et al., 1997 and the references therein; Nidzieko and Monismith, 2013), Morro Bay is a seasonally LIE characterized by an extended dry summer season (~April to November) with very little to no precipitation and freshwater inputs, and a shorter wet winter season (~December to March) with intermittent rainfall (annual average of approximately 50 cm with strong interannual variability, i.e., wet years and drought years, see Fig. 2) and freshwater inputs from the adjacent watershed. During the summer dry season, rainfall is rare and volumetric discharge rates from Chorro Creek are typically less than 0.1 m^3/s (average of 0.06 m^3/s during the study period). During the winter wet season, typical creek discharge rates during intermittent rainfall events range from 10 m^3/s to over 100 m^3/s (MBNEP, 2015).

Historical data on eelgrass spatial coverage up until 2003 were obtained from several different sources using a combination of field surveys and aerial photos (see MBNEP, 2017, Fig. 2a). Starting in 2004, eelgrass distributions were mapped periodically using aerial flights and multispectral aerial images obtained during low tides since most of the eelgrass in Morro Bay is intertidal (MBNEP, 2017). Following a guided classification methodology and preliminary classification, field-based surveys were conducted to verify substrate and vegetation types. Preliminary results from drone-based surveys conducted in 2017 and true color images showed close agreement with the 2017 aerial flight surveys. From 2007 to 2013, eelgrass went from 139 ha to less than 6 ha in 2013 with no apparent rebound.

Despite the overall decline, eelgrass beds near the mouth of the bay remain healthy through 2017 based on aerial surveys and in-situ monitoring (Fig. 1) and represent the only persistent eelgrass beds in Morro Bay. Moreover, since 2012, the Morro Bay National Estuary Program (MBNEP) and its partners have been conducting restoration outplanting of eelgrass with varying success (MBNEP, 2017). Between 2012 and 2014, the Morro Bay National Estuary Program (MBNEP) and its partners conducted several large-scale and bay-wide transplanting (22,924 planting units in 116 individual beds) and seeding efforts, but this combined effort had very little success with no impact on overall eelgrass area. A more recent small-scale outplanting effort in 2017 successfully transplanted eelgrass to a location closer to the mouth of the bay, but the outplanted beds in the back of the bay did not survive. The goal of this study is to develop a better understanding of current bay hydrodynamics and environmental conditions across gradients in eelgrass health and survival (e.g., going from the existing healthy beds near the mouth to the back bay areas that historically supported eelgrass populations). This work will inform restoration efforts and provide a better understanding of the role of hydrodynamics in maintaining alternative states in seagrass ecosystems.

2.2. Experimental setup

Oceanographic moorings were deployed throughout Morro Bay to assess spatial differences in environmental conditions and hydrodynamics across the gradient of eelgrass survival (Fig. 1, Table 1). Moorings were deployed from 29 June to 4 August 2016 during the summer dry season, during which the bay receives negligible freshwater inputs, to characterize low-inflow conditions. The moorings were located at three locations in the main channel of the bay (Fig. 1): a deeper location near the mouth of the bay (Bay Mouth; BM), one in the mid portion of the bay (Bay Center; BC), and one in the shallow back-bay region (Bay Head; BH). Each mooring was equipped with various instruments, depending on the site, measuring environmental conditions and oceanographic parameters including pressure (tidal height changes), velocity, conductivity (salinity), temperature, turbidity, chlorophyll-*a* (hereafter referred to as chlorophyll), and dissolved oxygen (DO) (see Table 1 for a detailed experimental setup description). Note that conductivity (salinity) was not directly measured at BH due to a lack of instrument availability.

Meteorological data, including local wind data, were obtained from measurements (15 min intervals) collected at the BH site. Historical precipitation data going back three decades were obtained from the California Irrigation Management Information System (CIMIS) station 52 (35.305442°N, 120.66178°W), which contained the longest and most complete record in the area. Historical dredging records going back three decades for Morro Bay were obtained from the Army Corps of Engineers (Joe Ryan, personal communication). Additionally, near-surface temperature measurements were obtained from long-term measurement sites at the mouth (2007–2017) and head (2007–2011) of the estuary (collocated with BM and BH in the present study), as well as a surface buoy (2007–2017) located on the shelf just offshore of Morro Bay (National Data Buoy Center 46011; 34.956°N, 121.019°W).

Scuba divers maintained moorings throughout the experiment with approximately weekly cleanings, and several small gaps of data were removed from further analyses due to biofouling or sensor issues (e.g., turbidity/fluorometer at BS reached sensor range limits likely due to macroalgae cover in the beginning of the experiment; the conductivity signal at BC started to generate data with spikes several times greater

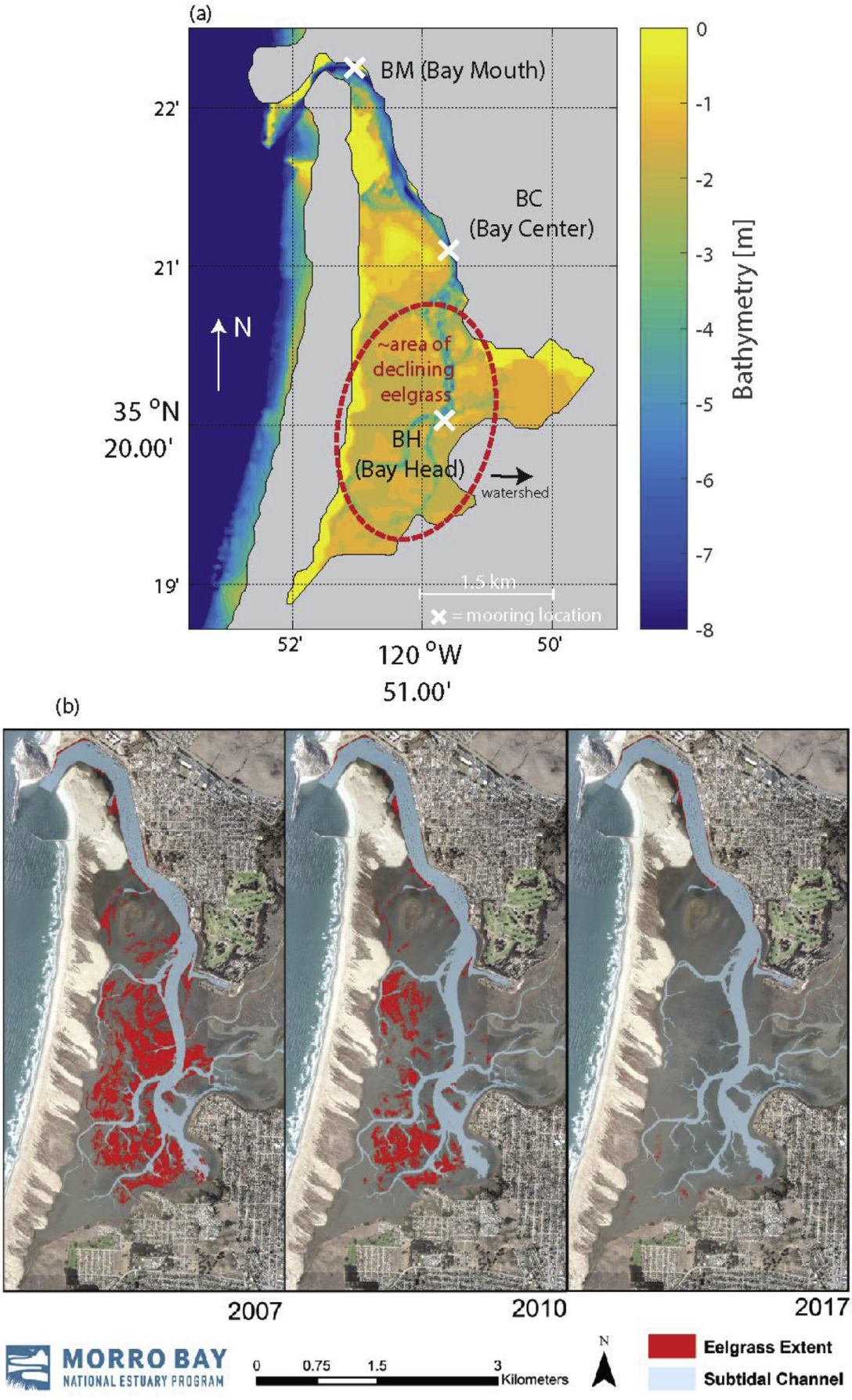

(caption on next page)

Fig. 1. (a) Bathymetry of Morro Bay and the location of oceanographic moorings (white x). The approximate area of extensive eelgrass loss in the mid-to back-bay region is denoted with a dashed red circle. (b) Eelgrass distribution in Morro Bay over time showing remaining eelgrass beds near the mouth and lost eelgrass beds in the back bay. Data were collected using aerial flights and multi-spectral imagery with field-based ground truth surveys (MBNEP, 2017). (For interpretation of the references to color in this figure legend, the reader is referred to the Web version of this article.)

than the background variability with large outliers, likely due to a clogged pump, so data after this event were removed; see Fig. 1). The current meters at BM and BC were leveled by divers to within 1° of the horizontal to minimize instrument tilt errors. A principal axes analysis was performed to rotate the velocity measurements into along-channel (AC) and cross-channel (XC), where positive AC denotes into the estuary (i.e., towards the back bay) and positive XC is 90° counterclockwise from positive AC. AC velocities were typically an order of magnitude larger than XC velocities. Surface layer effects were accounted for by removing velocity bins in the top 10% of the water column plus one extra bin based on the echo intensity values. All times referenced are in local time (Pacific Daylight Time).

2.3. Analysis methods

2.3.1. Horizontal Richardson number

The horizontal Richardson number was calculated to assess the influence of the longitudinal (i.e., along-channel) density gradients on the baroclinic circulation (e.g., Monismith et al., 2002),

$$Ri_x = \frac{\frac{\partial \rho}{\partial x} g h^2}{\rho u_*^2}, \tag{1}$$

where $\frac{\partial \rho}{\partial x} = 9.0 \times 10^{-5}\,\mathrm{kg/m^4}$ is estimated from the average density gradient between BM and BC, $g = 9.8\,\mathrm{m/s^2}$, $h = 6.0\,\mathrm{m}$ is computed as the average depth between BM and BC, and the friction velocity ($u_* = 1.5 \times 10^{-2}\,\mathrm{m/s}$), obtained from law of the wall boundary fits (see Section 2.3.4), is calculated as the average value from the law of the wall boundary layer fits at BM and BC.

2.3.2. Tidal excursions

Tidal excursions were calculated to approximate the typical displacement of a fluid parcel during a tidal cycle,

$$\xi(x_0, t) = \int_0^t <AC>(x_0, \tau) d\tau, \tag{2}$$

where x_0 is the point where the depth-averaged along-channel velocity ($<AC>$) is measured (either BM or BC), and t is the time of interest. We note that this Eulerian-derived tidal excursion is a first-order approximation since the true (i.e., Lagrangian) excursion of a fluid parcel will be affected by spatial differences in velocity along the channel. Due to the observed subtidal velocities and to better estimate the magnitude of the excursions during a typical tidal cycle, net tidal excursions were high-pass filtered (33 h half amplitude period; pl66 filter, Beardsley et al., 1985).

2.3.3. Salinity budget

The defining dynamical character of LIEs that exhibit hypersaline basins is a long residence time relative to the time scale of evaporative surface fluxes. To investigate this, we follow the approach of Largier et al. (1997) by starting with the longitudinal salt balance:

$$\frac{\partial S}{\partial t} = \frac{\partial}{\partial x}\left[K_x \frac{\partial S}{\partial x} + \frac{Ex}{H} S\right], \tag{3}$$

where $S(x,t)$ is the salinity, $E(t)$ is the evaporation rate, $H(x)$ is the water depth, x is the longitudinal distance from the estuary head (i.e., $x = 0$ at the head in the back bay, with positive x seaward from the head), and $K_x(x,t)$ is the longitudinal salt diffusivity. Precipitation and stream inflow were assumed to be zero, given the low-inflow dry season in California (see also Largier et al., 1997). In the above equation, for

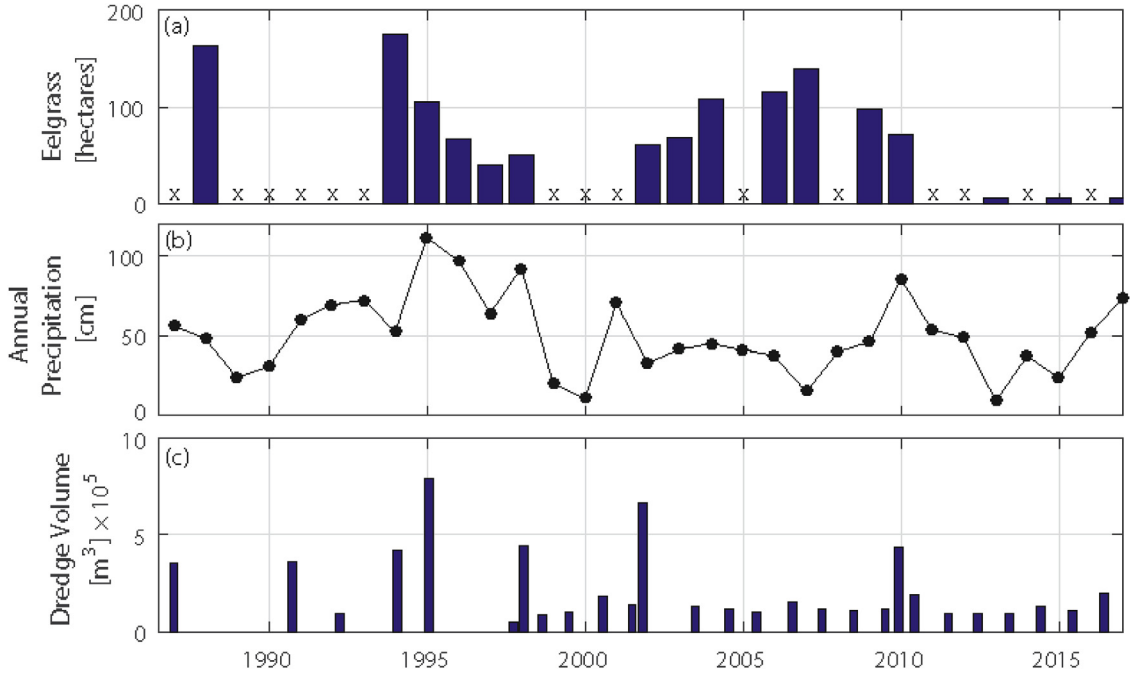

Fig. 2. Historical time series of (a) eelgrass coverage, (b) annual precipitation, and (c) dredging volume. The small "x" in panel (a) denotes that data were not collected during that particular year. Dredging data are plotted according to the dredge start date. All dredging activity occurred over a period of less than three months except for the following dates (start month and year to end month and year): Dec 86 - Apr 87, Jan 95 - Apr 96, Jan 98 - Apr 98, Oct 01 - Jul 02, May 05 - Jun 06.

the salt content in the basin to remain constant (i.e., steady-state), the advective salt flux into the basin from evaporation needs to be balanced by a diffusive salt flux out of the basin (i.e., seaward), thus requiring the horizontal gradient to decrease away from the head (i.e., $\frac{\partial S}{\partial x} < 0$, a hypersaline basin).

Following Largier et al. (1997) we assume a dry-season steady-state and scale the longitudinal diffusivity according to Prandtl's mixing length model as, $K_x = kx^2$, where k is a constant determined from the model fit described below and x is the longitudinal distance from the estuary head. This follows from the idea that the velocity and length scales of tidal motion scale with x since dispersion is dominated by tidal motions in the absence of density-driven vertical exchange (cf. Largier et al., 1997). Under these assumptions, Equation (3) yields the following analytical expression for the salinity decrease with distance from the head (i.e., increase of salinity with distance from the ocean/mouth):

$$S = S_o\left(\frac{x}{L}\right)^{-\frac{E}{kH}}, \tag{4}$$

where $S_o = 33.70$ is the average salinity calculated at the Bay Mouth site (BM), $H = 4.8$ m is calculated as the average depth at the Bay Center (BC) site representative of the average channel depth in Morro Bay, and $L = 6.0$ km represents the distance from BM to the head of the estuary (i.e., just south of BH). The average evaporation rate over the experiment ($E = 4.1$ mm/day) was determined from, $E = Q_L/(L_e\rho_w)$, where Q_L is the latent heat flux calculated following the bulk formula in Rosenfeld et al. (1994) (see also Suanda et al., 2011; Walter et al., 2017), L_e is the latent heat of evaporation, and ρ_w is the density of water.

Using average salinities at BM and BC, as well as the inferred average salinity at BH (see below), the data were fit to Equation (4) using a nonlinear least squares regression. At BH the average salinity was inferred (S = 34.0) by calculating the average temperature at BH and using the TS diagram at BC to identify the back-bay water mass and salinity with this particular temperature (see dashed lines in Fig. 6b). From the model fit, the constant k was determined and used to calculate $K_x(x) = kx^2$ (Fig. 7b, solid line). Modeled diffusivity estimates were compared with diffusivities calculated by assuming a steady-state balance in Equation (1) between the diffusive salt flux and the advective salt flux due to evaporation:

$$K_x\frac{\partial S}{\partial x} \sim -\frac{ExS}{H} \rightarrow K_x \sim -\frac{ExS}{H}/\frac{\partial S}{\partial x}. \tag{5}$$

where $\frac{\partial S}{\partial x}$ was numerically estimated at each site using finite differences.

An estimate of the flushing time, which is defined as the time needed to completely diffuse the hypersalinity out of the system, is given by the following expression (Largier et al., 1997):

$$\tau_{flush} = \frac{(S - S_o)x}{-K_x\frac{\partial S}{\partial x}}, \tag{6}$$

where $\frac{\partial S}{\partial x}$ was calculated from Equation (4). Flushing time estimates from the model fit were compared to observed residence times (i.e., age of a water parcel in the basin) determined from a bulk (Lagrangian) salt balance,

$$\tau_{res} \sim \frac{(S - S_o)H}{ES_{avg}}, \tag{7}$$

where $S_{avg} = \frac{S + S_o}{2}$ is a measure of the Lagrangian average salinity (Largier et al., 1997).

2.3.4. Boundary layer dynamics

For shallow tidal flows, the development of near-bed turbulence controls flow and transport processes, including vertical mixing and sediment resuspension events. For a well-developed turbulent boundary layer, the law of the wall describes mean velocity profiles,

$$U(z) = \frac{u_*}{\kappa z}\ln\left(\frac{z}{z_o}\right), \tag{8}$$

where $\kappa = 0.41$ is Von Kármán's constant, u_* is the friction velocity, and z_o is the roughness height. Using Equation (8), linear regressions between 10-min averaged along-channel velocities (U) throughout the water column and $\ln(z)$ were performed at BM and BC to yield estimates of the friction velocity (u_*) and roughness height (z_o) during each 10-min time period. To ensure a well-defined logarithmic profile, only unidirectional profiles having a coefficient of determination (R^2) > 0.75 were used for further analysis. This restriction ensures a 95% confidence interval for the friction velocities of ± 38% (Gross and Nowell, 1983; Cheng et al., 1999).

The drag coefficient was determined from the slope of the regression between the friction velocity squared and the reference velocity squared (e.g., Cheng et al., 1999; Reidenbach et al., 2006):

$$C_d = \frac{u_*^2}{U_0^2}. \tag{9}$$

Linear regressions were performed for both the flood and ebb currents at BM and BC. Using the friction velocity estimates, bed shear stresses, which represent the force per unit area exerted on the bed by the flow, were calculated as,

$$\tau = \rho u_*^2. \tag{10}$$

3. Results and discussion

3.1. General observations

Local winds in the back bay were primarily aligned in the east/west direction and showed a distinct diurnal signal, with eastward sea breezes peaking in the early evening (Fig. 3a). Tides in the bay were mixed semidiurnal and exhibited spring-neap variability (Fig. 3b). The tidal height (h'), defined here with the time-mean removed, at BM and BC were nearly identical and almost perfectly in phase, a direct consequence of the shortness of the estuary. The dominant motions at BM and BC were tidally driven and exhibited a strong semidiurnal signal with fortnightly variability driven by the spring-neap tidal cycles (Fig. 4). The dominant direction of velocities was along-channel (i.e., the major axis of the principal-axes analysis), with along-channel velocities an order of magnitude larger than cross-channel velocities. Along-channel velocities also displayed a typical barotropic vertical structure with no zero crossings (i.e., absence of baroclinic motions) (Fig. 4a). The depth-averaged along-channel velocities ($< AC >$, where the brackets denote a depth-averaged quantity) exhibited strong asymmetries at the BM site with flood velocities (max speed = 0.78 m/s) much greater than ebb velocities (max speed = 0.38 m/s) (Fig. 4b). At the BC site, velocities displayed a slight ebb-dominance (max flood speed = 0.61 m/s, max ebb speed = 0.78 m/s) (Fig. 4b). The subtidal (33 h half amplitude period; pl66 filter, Beardsley et al., 1985) velocities at BM show significant subtidal means directed into the bay (i.e., positive) that are modulated over the spring-neap cycle, while BC shows minimal subtidal velocities (Fig. 4c). Comparison of the velocities at both sites with the changing tidal elevation shows that these quantities were in near quadrature (90° out of phase – i.e., maximum currents take place when $\frac{\partial h}{\partial t}$ is maximum), which is typical of short, shallow estuaries in California (Nidzieko, 2010).

Along the U.S. West Coast, higher-high water precedes lower-low water due to the phasing of the diurnal and semidiurnal tidal constituents (cf. Nidzieko, 2010). In this case, the tide entering an estuary should be ebb-dominant with respect to rise and fall duration, resulting in asymmetric ebb-dominated velocities; however, local bathymetry and other site-specific factors (e.g., river inflow/baroclinic motions) can lead to significant internal distortions within the estuary, resulting in site-specific responses and velocity asymmetries (cf. Nidzieko, 2010;

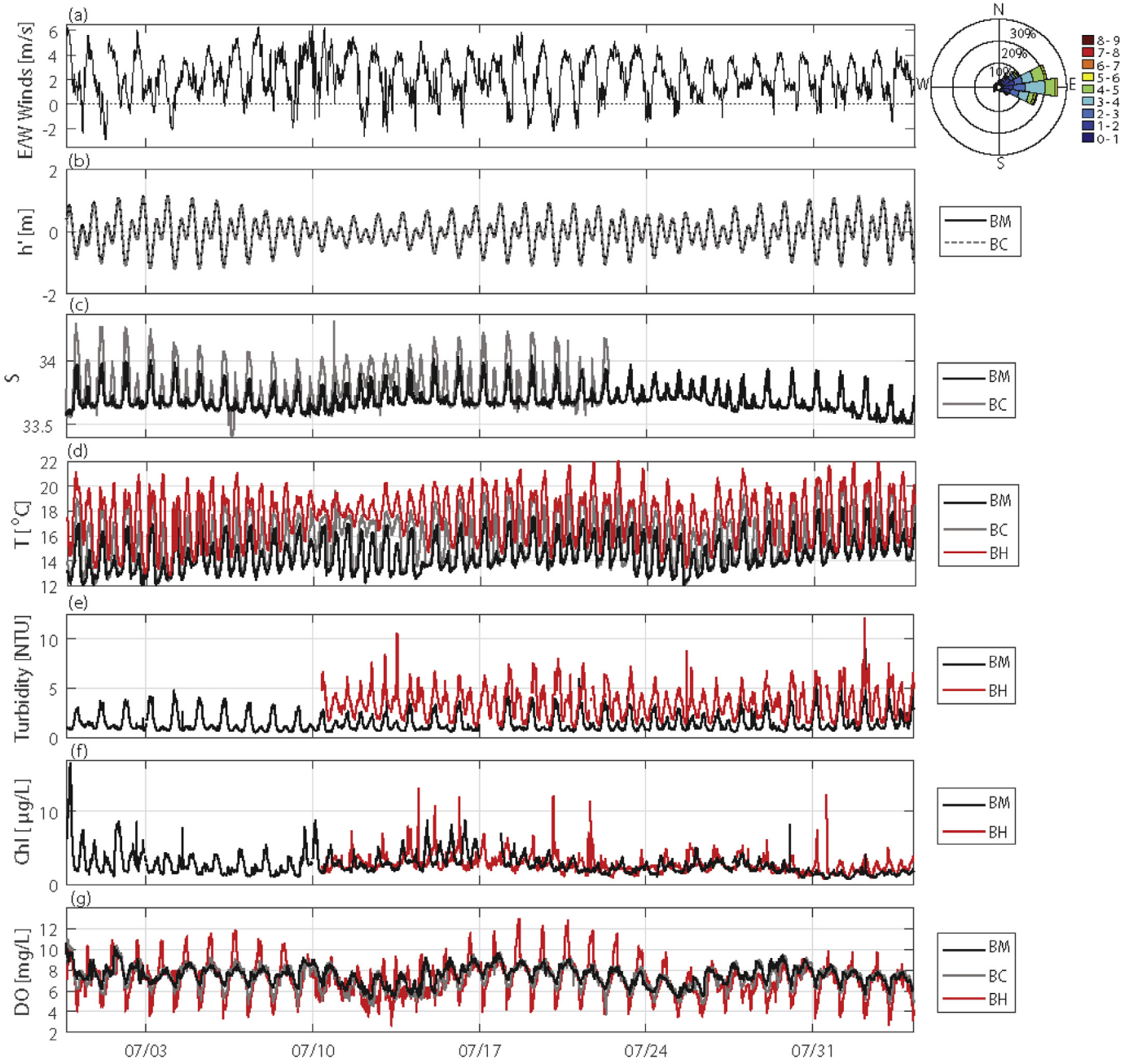

Fig. 3. Time series (day/month in 2016) of (a) local east/west winds (positive = eastward), shown with the local wind rose (oceanographic orientation – directionality indicates wind vector direction), (b) tidal height with the time-mean removed, (c) salinity, (d) temperature, (e) turbidity, (f) chlorophyll, and (g) dissolved oxygen at several bay locations (colors in panels b–g represent Bay Mouth (BM) – black; Bay Center (BC) – gray; Bay Head (BH) – red). Data gaps are due to biofouling or sensor issues. (For interpretation of the references to color in this figure legend, the reader is referred to the Web version of this article.)

Nidzieko and Ralston, 2012). To investigate the observed asymmetries, we calculated the skewness of the tidal height time derivative ($\frac{\partial h}{\partial t}$) following Nidzieko (2010). The skewness, which quantifies duration asymmetry in the rise and fall of the water level, was negative, indicating a tendency for ebb-dominated velocities. The skewness of the along-channel velocities at BM and BC was positive and negative, respectively, indicating flood-dominated and ebb-dominated regimes. This suggests that the flood-dominated velocities at BM were likely driven by local bathymetry since asymmetries in tidal currents produced from bathymetry generally do not show up in the tidal elevation record and baroclinic motions were not present in the data (cf. Nidzieko, 2010). Moreover, the generation of residual subtidal circulation has been shown to depend on a variety of factors and forcing including bed roughness, cross-sectional area and width, and rectification of tidal velocities (e.g., Li and O'Donnel, 2005; Burchard, 2011). The mooring at BM was placed in the center and deepest part of the channel, but significant lateral variations in bathymetry, the presence of local curvature, and other factors (lateral flow effects, bed roughness differences) may have led to the observed subtidal flow field. This effect will be further investigated in future modeling studies.

Salinity, temperature, and DO at BM generally showed little to no vertical differences, indicative of well-mixed waters and strong tidal mixing (see also Section 3.2). Salinity showed a semidiurnal signal with stronger variability at the mid-bay site (BC) compared to the mouth site (BM) (salinity was not measured at BH; Fig. 3c; see also section 3.2). Salinities at BC were also greater than those at BM, which follows the

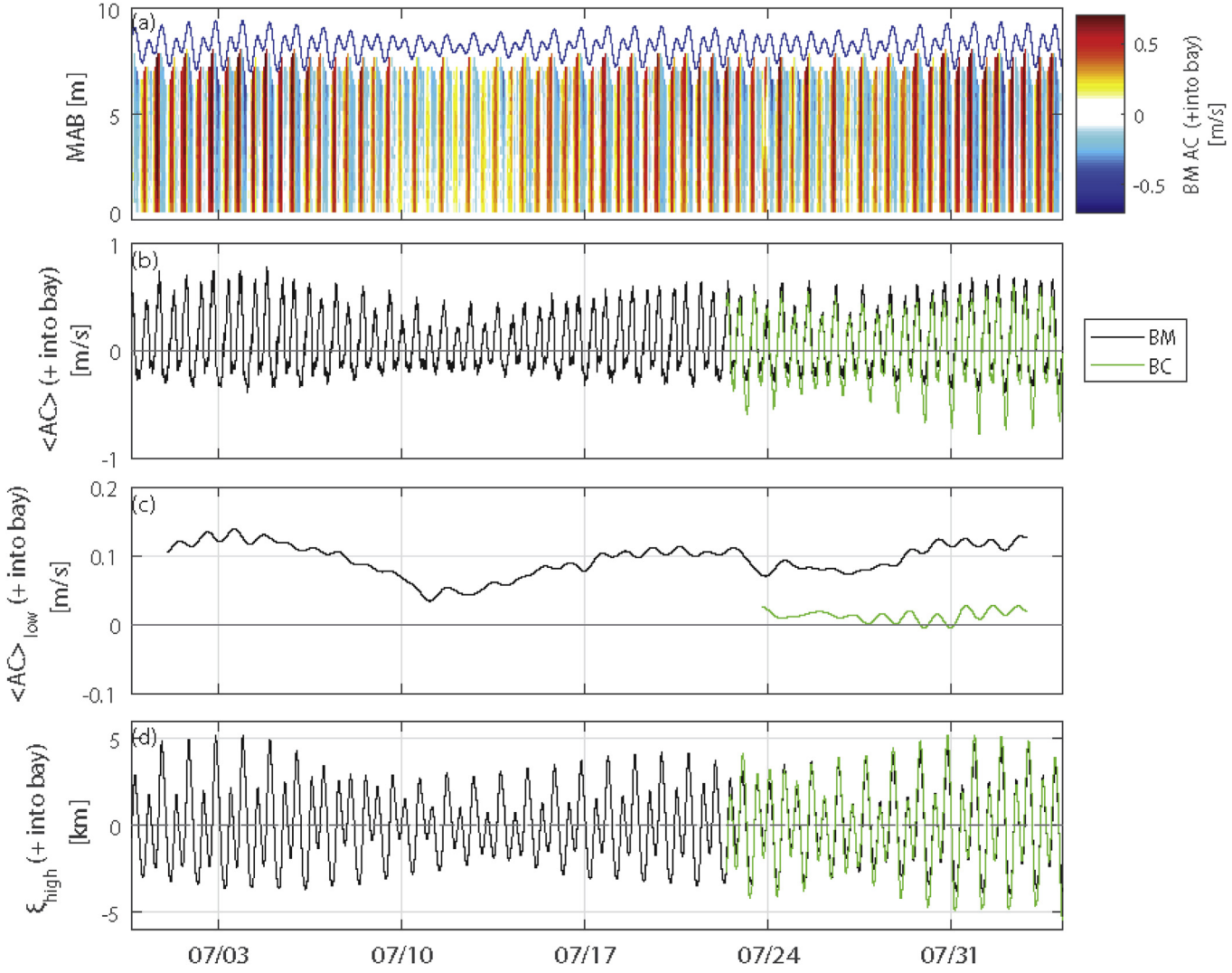

Fig. 4. Time series of the (a) along-channel (AC) velocity at various depths at Bay Mouth (BM), (b) depth-averaged along-channel velocity at BM (black) and Bay Center (BC, green), and (c) subtidal (33 h low-pass filter) depth-averaged along-channel velocity at BM (black) and BC (green), and (d) high-pass filtered (33 h) tidal excursions at BM (black) and BC (green). The solid blue line in panel (a) denotes the sea surface height. For both the velocities and tidal excursions, a positive value denotes into the bay/towards the head, while a negative value denotes out of the bay/towards the mouth. BC velocities were only measured from 22 July onward. (For interpretation of the references to color in this figure legend, the reader is referred to the Web version of this article.)

definition of a hypersaline estuary [$(\overline{S}_{BC} - \overline{S}_{BM}) > \sigma_{BM}$, where an overbar denotes a time-average ($\overline{S}_{BC}$ = 33.80, $\overline{S}_{BM}$ = 33.70) and σ_{BM} = 0.09 denotes the standard deviation of the salinity at BM, see Largier (2010)]. Spatially, strong differences in temperature occur throughout the bay with colder waters at the ocean-forced mouth and increasingly warmer waters in the shallower back-bay portions (Fig. 3d), indicative of a hyperthermal estuary (Largier, 2010). In the summer period, estuarine temperatures rise due to solar heating, but ocean temperatures remain cooler due to seasonal wind-driven coastal upwelling in this region (cf. Walter et al., 2018). In addition to significantly warmer waters in the back bay compared to the other sites, tidally-driven temperature fluctuations were much larger with temperature changes as large as 8 °C over a 6-h period at BH.

For the water quality parameters, turbidity also displayed semi-diurnal variability, with the turbidity signal peaking during the low tides (Fig. 3e; see also Section 3.4). Turbidity values in the back bay were consistently higher than those measured near the mouth. The chlorophyll time series was more irregular, with intermittent peaks occurring throughout the record, particularly in the back bay (Fig. 3f). Dissolved oxygen displayed a regular diurnal cycle at all sites with peaks in the early evening (~15:00-20:00) and minimums in the early morning (~05:00-08:00) (Fig. 3g). DO levels in the back bay displayed much stronger diurnal variability and more than double the daily range compared with the mouth. Moreover, early morning minimums often dropped below 4.6 mg/L, the hypoxic threshold designated by Vaquer-Sunyer and Duarte (2008) for marine benthic organisms. The large diurnal ranges observed in the shallower back bay are likely due to production of oxygen by macroalgae (e.g., expanses of red and green algal species in the back bay that vary seasonally and year to year, cf., MBNEP, 2013) and phytoplankton during the day and community respiration in the evening (including microbial respiration) (Moore, 2004). Macroalgae likely dominate the production during the day given that chlorophyll concentrations did not show a strong diurnal signal. Moreover, recent surveys showed a higher percentage of carbon in soil samples from the back bay relative to the mouth of the bay (E. Aiello and J. Yost, personal communication), suggesting that microbial respiration may be contributing to some of the low DO values in the shallow back bay, although this is a hypothesis that warrants further research.

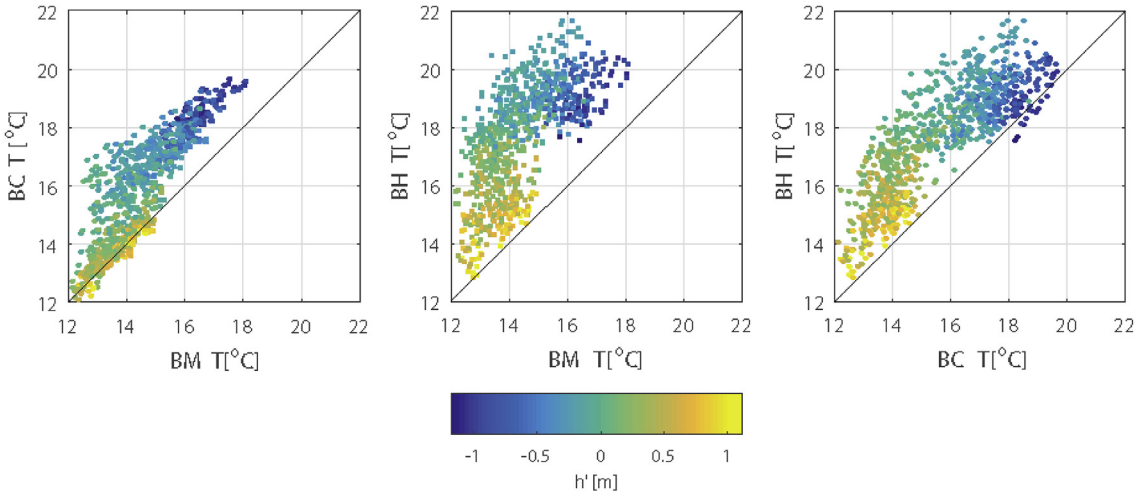

Fig. 5. Temperature scatter plots (1 h averages) between (a) Bay Mouth (BM) and Bay Center (BC), (b) BM and Bay Head (BH), and (c) BC and BH. The colors indicate the tidal height at BM, where the time-mean has been removed. A one-to-one line is plotted for reference (black line) indicating when the two locations have the same temperature. (For interpretation of the references to color in this figure legend, the reader is referred to the Web version of this article.)

3.2. Bay water masses

Spatial differences in temperature throughout the bay are highlighted in Fig. 5, which shows scatter plots of temperature at BM, BC, and BH with the colors denoting the tidal height with the time-mean removed (*h*'). A comparison between the mouth (BM) and mid bay (BC) reveals similar cold temperature waters during the highest tidal elevations, indicative of waters originating from the ocean (Fig. 5a). However, during mid-range tides ($h' \sim 0$) and the lowest tidal elevations, BC waters were several degrees warmer than BM. A comparison of the mouth (BM) waters to the back-bay (BH) waters shows that the waters in the back bay were significantly warmer than the mouth across all tidal elevations (Fig. 5b). This is particularly evident during the mid to low range of *h*' where temperatures differences between the two sites were more than 5 °C. When comparing BC and BH (Fig. 5c), the waters at BH were consistently warmer except during the lowest tides when both sites reached the same high temperatures. These findings demonstrate the presence of a strong thermal gradient between the mouth (BM) and head (BH). Colder bay-mouth waters were transported to the mid-bay site during higher tides and warmer back-bay (head) waters were transported to the mid-bay site during lower tides, but the mouth and head exhibited minimal exchange.

Further delineation of the different water masses is shown in Fig. 6, which shows temperature-salinity (TS) diagrams for the mouth and mid-bay [conductivity (salinity) was not directly measured in the back bay]. The mean (standard deviation) of temperature at BM, BC, and BH were 14.42 °C (1.28 °C), 15.63° (1.90 °C), and 17.62° (1.90 °C), respectively. For salinity, the mean (standard deviation) at BM and BC were 33.70 (0.09) and 33.80 (0.17), respectively. During the lowest tides, BM and BC showed similar water mass structure composed of colder and less saline waters. The TS parameter space at BC showed a distinct water mass composed of warmer and saltier waters that was not observed at BM. This water mass was measured during the lowest tidal elevations, which indicates an origin from the back portions of the bay. The average temperature measured at BH is shown as a dashed horizontal line in Fig. 6b for reference. The TS diagrams corroborate the idea that the mid-bay site acts as a transition zone between the mouth and back bay water masses, with minimal exchange between the mouth and back bay. The mouth water mass is colder and less saline relative to the warmer and more saline back bay water mass (i.e., a hyperthermal, hypersaline estuary, cf. Largier, 2010). However, despite the hypersaline conditions, the gradient in temperature still maintained larger densities at BM compared to BC. This situation has been termed a "thermal estuary" (cf. Largier, 2010; Largier et al., 2013). Moreover, the

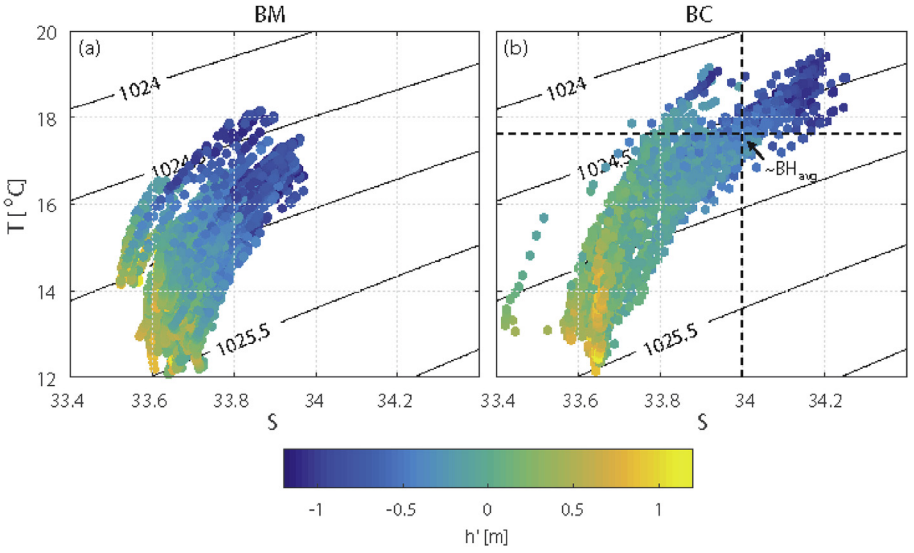

Fig. 6. Temperature-salinity (TS) diagrams at Bay Mouth (BM) and Bay Center (BC) showing water mass composition. The colors indicate the tidal height at BM where the time-mean has been removed, while the diagonal lines denote lines of constant density [kg/m^3]. In panel (b), the dashed black lines denote the average measured temperature (17.62 °C) at Bay Head (BH) and an estimate for the average salinity (34.0). (For interpretation of the references to color in this figure legend, the reader is referred to the Web version of this article.)

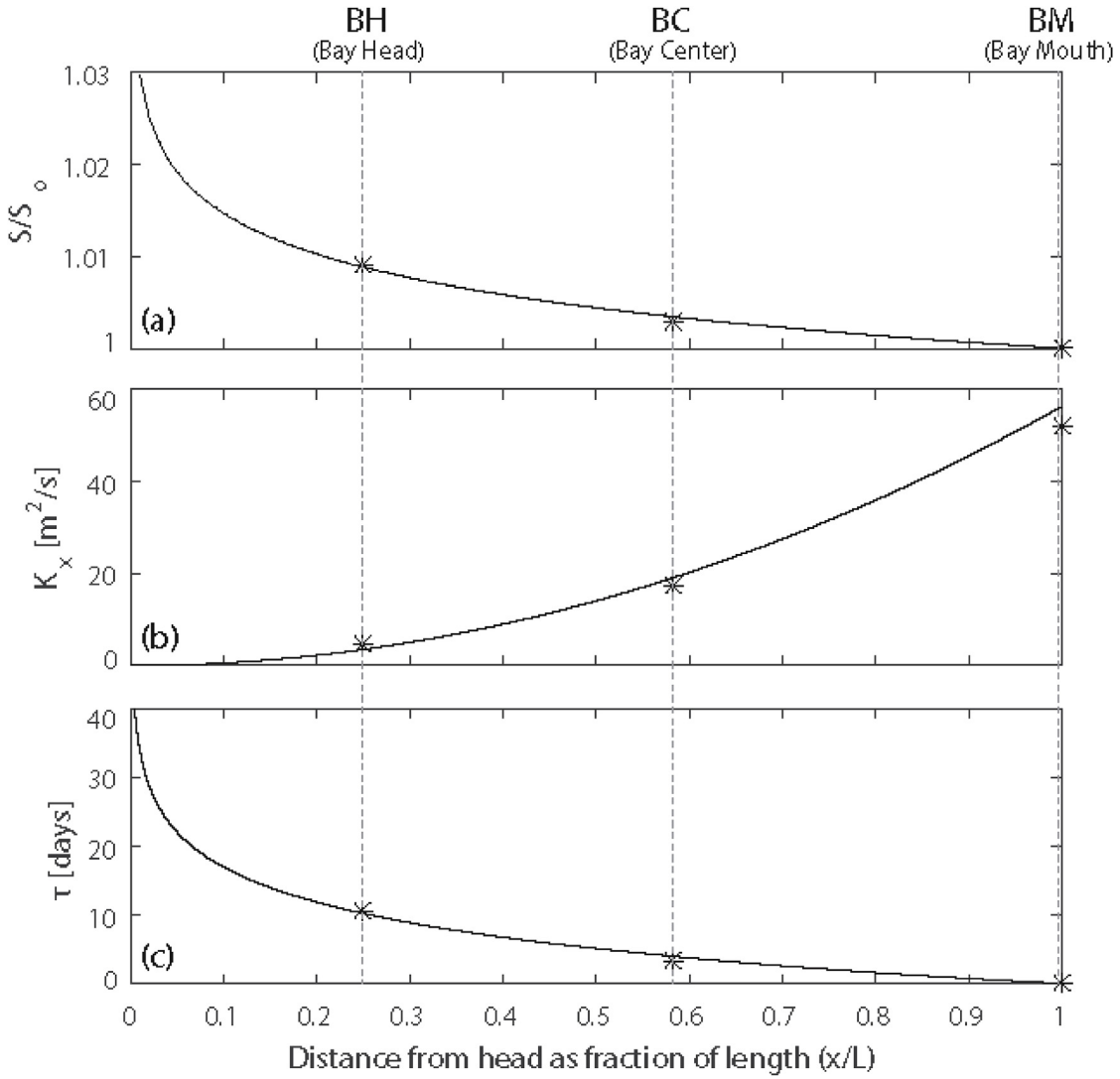

Fig. 7. Longitudinal changes in the (a) salinity normalized by the salinity at the Bay Mouth (BM) (observed as symbols, model fit from Equation (4) as solid line), (b) longitudinal diffusivity (observed calculated from Equation (5) as symbols, model fit from $K_x = kx^2$ as solid line) and (c) flushing/residence time (observed residence times from Equation (6) as symbols, and modeled residence times from Equation (7)). All quantities are plotted as a function of distance from the estuary head as a fraction of the estuary length, where BH, BC, and BM mooring locations are labeled on top of panel (a) and highlighted with dashed gray lines on each subplot.

horizontal Richardson number calculated using average values between BM and BC (Equation (1); see Section 2.3.1) was equal to 0.02 and approached zero during the strongest flows, indicating that mixing was strong and that gravitational circulation and stratification were not important for the flow dynamics in the estuary during this time period.

Tidal excursions displayed strong spring-neap variability with displacements up to 5 km during spring tides (i.e., nearly equal to the ~5.5 km distance between BM and BH) and approximately 2–3 km or less during neap tides (e.g., approximate distance between BM and BC) at both sites. That is, waters at BM will be mainly oceanic, while those at BH will be older bay waters. This finding corroborates the observed water mass relationships described previously. Moreover, this suggests that BM and BH were essentially cutoff from one another except during the strongest spring tides. This is explored further in Section 3.3 with the calculation of residence and flushing times throughout the bay.

3.3. Salinity budget

Fig. 7a shows the average salinity (symbols) with distance from head (i.e., going from BH to BC to BM), as well as the model fit (solid line) from the longitudinal salt balance (Equation (4)). The model fit highlights the hypersaline conditions in the bay and decreasing salinities with distance from the head. From the model fit, the constant k was determined and used to calculate the longitudinal salt diffusivity $K_x(x) = kx^2$ (Fig. 7b, solid line). Modeled diffusivity estimates (solid line) agree well with diffusivities calculated (symbols) by assuming a steady-state balance between the diffusive salt flux and the advective salt flux due to evaporation (Equation (5)). As expected for a hypersaline system, flushing times are largest (i.e., slowest) near the head of the estuary and decrease substantially towards the mouth (Fig. 7c, solid line). These values agree well with observed residence times (i.e., age of a water parcel in the basin) calculated using Equation (7). Calculated flushing and observed residence times at BH were approximately two weeks and increased substantially to over 30 days closer to the head of the estuary. Closer to the mouth, flushing and residence times were on the order of days. While other processes may be affecting these estimates (cf., Largier et al., 1997), they support the idea that waters near the head of the estuary are the oldest waters. These findings also corroborate the existence of distinct water mass systems with minimal exchange. Moreover, previous estimates of flushing times in Morro Bay using tracer releases in a numerical model during low-inflow conditions also found regions near the head had flushing times on the

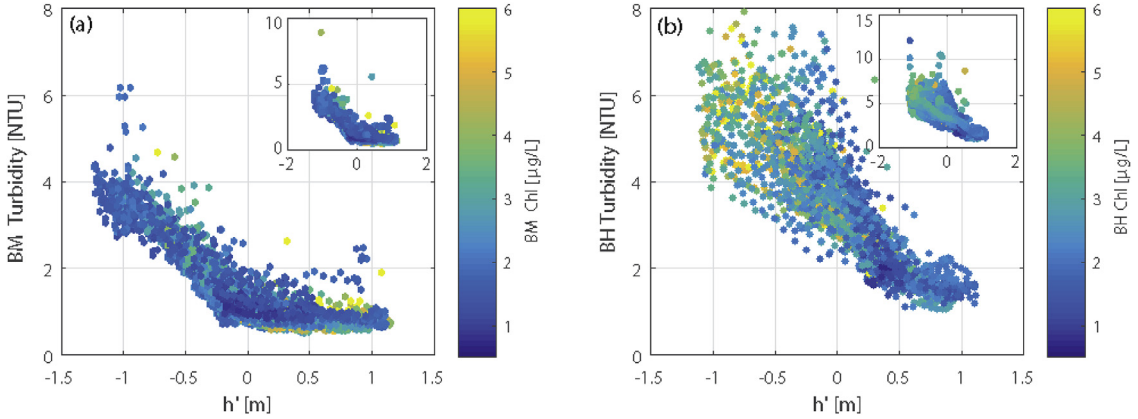

Fig. 8. Turbidity as a function of the time-mean removed tidal height (h') at BM at (a) Bay Mouth (BM) and (b) Bay Head (BH). The colors denote the chlorophyll concentration (colorbar) at the respective site. The inset panel in the top right corner of each plot shows the same scatter plot zoomed out to highlight outliers that were not included in the larger plots. (For interpretation of the references to color in this figure legend, the reader is referred to the Web version of this article.)

order of two weeks or more (Tetra Tech, 1999; their Figs. 5–1). These results highlight that during the low-inflow dry season, evaporative surface fluxes drive hypersaline conditions and the decoupling of the bay-mouth and back-bay waters for several weeks at a time.

3.4. Turbidity and boundary layer dynamics

Turbidity data were compared at the bay-mouth (BM) and back-bay sites (BH). Generally, both sites displayed the largest turbidities during the lowest tides, with turbidities in the back bay elevated relative to the mouth (Fig. 3e). There was little correspondence between the turbidity and the near-bottom velocities or the local diurnal wind forcing, respectively. Fig. 8 shows the turbidity as a function of the time-mean removed tidal height (h') at both sites, where the colors also denote the local chlorophyll concentration at each site. Both sites show a constant turbidity at larger tidal heights, with a distinct transition to approximately linearly increasing turbidities with progressively lower tidal heights. This transition between constant and linearly increasing turbidities occurs at lower time-mean removed tidal heights for the bay-mouth site ($h' \sim 0$) compared to the back-bay site ($h' \sim 0.5$). This is significant since the back-bay site will experience increased turbidities over longer periods of time (i.e., greater percentage of tidal phases). Moreover, not only were the turbidities at the lowest tidal heights in the back bay nearly double those near the mouth (~8 NTU at BH and ~4 NTU at BM), but during the high-tide periods of constant turbidity, the back-bay turbidity values were also larger (~1.5 NTU at BH and ~0.75 NTU at BM), indicative of larger background levels. Additionally, during the lowest tides with the largest turbidities, chlorophyll concentrations in the back-bay were slightly elevated (~4–6 µg/L at BH, ~2 µg/L at BM; colors in Fig. 8).

Fig. 9a shows the friction velocity as a function of the mean velocity at 1.1 m above the bottom (hereafter referred to as the reference velocity, U_0). Both the BM and BC sites showed increases in the friction velocity with increasing mean reference velocity, particularly for flood (positive U_0) currents. Additionally, during ebb (negative U_0) currents, friction velocities were substantially enhanced relative to flood currents for the same velocity magnitude, indicating strong asymmetries in the boundary layer characteristics.

The calculated drag coefficients for flood currents at BM and BC were 0.0032 ± 0.0001 and 0.0054 ± 0.0002, respectively, where the uncertainty bounds were determined from 95% confidence intervals on the slope estimates from the linear regression. These drag coefficient values are comparable to those expected for flow over sand and mud (Gross and Nowell, 1983; Monismith et al., 2005; Reidenbach et al., 2006). The ebb current drag values at BM and BC were nearly an order of magnitude larger at 0.027 ± 0.003 and 0.036 ± 0.007, respectively. Similar flood/ebb asymmetries were found using the roughness length (z_0) from the law of the wall fits to estimate the drag coefficient (cf. Cheng et al., 1999). Cheng et al. (1999) observed variations in the roughness length with tidal velocity and hypothesized that this was driven by sediment transport and a moving bed since the hydrodynamic roughness depends on the physical grain composition, hydrodynamic form drag, and the movement of sediment. Variations in the drag coefficient between sites and current directionality were likely driven by a combination of the movement of sediment (e.g., increased turbidities observed during the lowest tidal heights following strong ebb velocities, see Fig. 8) and local upstream bathymetry (e.g., bedforms, patchy vegetation, channel shoals, and other irregularities) (Cheng et al., 1999; Lacy and Wyllie-Echeverria, 2011; Walter et al., 2011; Hansen and Reidenbach, 2012, 2013).

Fig. 9c and d shows histograms of the bottom shear stresses for BM and BC, respectively. Relative to BM, measured stress distributions at BC contained a greater percentage of large shear stress events (i.e., longer tail in Fig. 9d). These large shear stress events are largely observed during ebb tidal currents (e.g., see Fig. 9b). Interestingly, the turbidity showed little to no correspondence with the near-bottom velocity, despite the dependence of the friction velocity, and hence shear stresses, on near-bed velocities. This indicates that local resuspension in the channel is unlikely the main source for the elevated turbidities observed in the channel. Rather, as discussed previously, turbidity demonstrated a strong dependence on the local tidal height (e.g., constant turbidity at higher tides and linearly increasing turbidities with lower tides after a transition point, Fig. 8).

It is likely that turbidity levels increase at the channel observation sites following the draining of the adjacent intertidal flats into the main channel during the transition to low tides. When the intertidal areas become inundated during high tides and then drain with the falling of the tide, local shear-driven resuspension in the intertidal flats and the subsequent transport of fine sediment and organic/inorganic matter (including microalgae given the positive relationship between turbidity and chlorophyll at low tides at BH, Fig. 8) from the intertidal flats [qualitatively a combination of mud and fine grains (sand/silt)] to the main channel likely occurs. The contribution to suspended matter in the channel appears to be dominated by transport from the adjacent flats and shoals, which peaks during low tides, as opposed to local resuspension in the channel. Chou et al. (2018) observed a similar effect in South San Francisco Bay where the transport of sediment from shoals into the adjacent channel, which peaked during low-water, was comparable to local resuspension in the channel. This phenomenon is likely amplified in the back portions of the bay (e.g., elevated turbidities at BH relative to BM, Fig. 8) given the proximity to large expanses of largely unvegetated intertidal flats, which were previously dominated

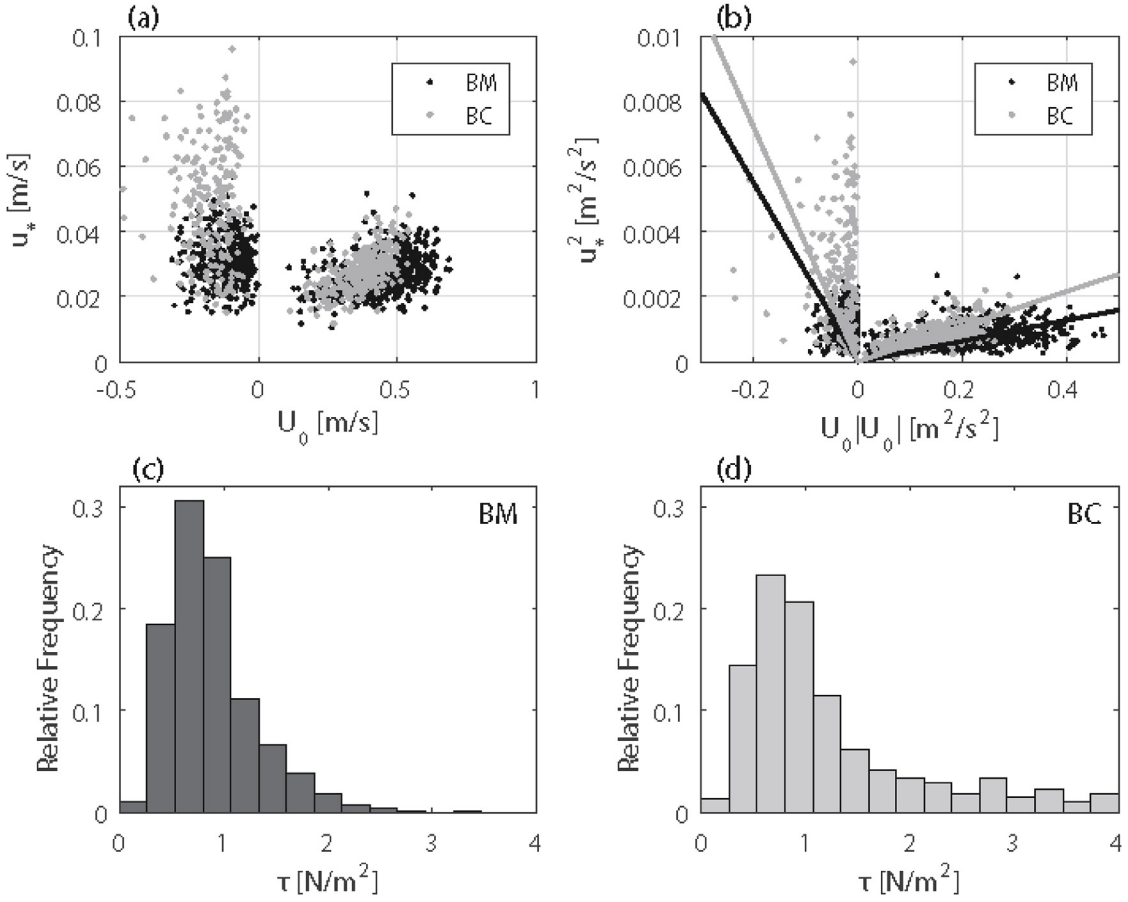

Fig. 9. (a) Friction velocity (u_*) estimated from the log-law fits as a function of the near-bed along-channel reference velocity (u_o) at the Bay Mouth (BM – black) and Bay Center (BC –green) sites. (b) Same as (a) but squared quantities (absolute value used to preserve sign on x-axis). The linear regression is shown for the flood (positive) and ebb (negative) velocities at each site (solid lines), where the slope of this fit represents the drag coefficient (C_d). Panels (c) and (d) show histograms of bed shear stresses at BM and BC, respetively. Histograms are normalized to show the relative frequency in each bin such that the sum of the bins is equal to one.

by eelgrass meadows (Fig. 1).

3.5. Implications for eelgrass

Existing bay hydrodynamics drive strong spatial differences in environmental conditions throughout the bay during the summer, low-inflow season. The mouth of the bay, which retained healthy and resilient eelgrass beds, was characterized by regular exchange with the adjacent ocean and short flushing times. Waters at this site were colder, less saline, more oxygenated, and less turbid when compared to other regions of the bay. The back of the bay, on the other hand, contained waters that were significantly warmer, more saline, less oxygenated, and more turbid, with longer flushing times. The weak exchange between the two sites acts to decouple these two regions of the bay, with the middle portions of the bay acting as a transition zone between the two water masses.

The environmental conditions in the back bay (long flushing times, increased temperatures, changing salinities, increased turbidity, and near hypoxic conditions in the channel where the measurements were taken) have all been identified as significant stressors, often acting synergistically with one another, on seagrass systems (Bulthuis, 1987; Moore et al., 1996, 1997; 2012; Short and Wyllie-Echeverria, 1996; Zimmerman et al., 2001; Greve et al., 2003; Orth et al., 2006; Collier and Waycott, 2014; Kaldy, 2014). For example, turbidity plays a critical role in the health and survival of eelgrass, given the need for the availability of light for photosynthesis (Moore et al., 1996, 1997; 2012; Zimmerman et al., 2001). In low-light environments, seagrass growth decreases as temperature increases (Bulthuis, 1987; Moore et al., 1997 and the references therein; Collier and Waycott, 2014). Globally, there are a number of studies of eelgrass response to temperature in different regions, and generally increases in temperature negatively impact eelgrass (Greve et al., 2003; Collier and Waycott, 2014; Kaldy, 2014; Kaldy, 2014; Moore et al., 2014; Beca-Carretero et al., 2018). However, optimal temperature ranges and responses are highly region and site specific. Generally, in high temperature environments, seagrasses are more vulnerable to wasting disease and low meristematic oxygen content, and in extreme cases, die-offs (Greve et al., 2003; Collier and Waycott, 2014; Kaldy, 2014). The existing environmental conditions in the back bay may have contributed to repeated, failed large-scale restoration attempts in this region of the bay (MBNEP, 2017). As mentioned earlier, in more recent transplant efforts from 2017, plots in the back portions of the bay did not survive (E. Aiello and MBNEP, personal communication). Further, it is clear that seasonality can affect restorative outplanting of eelgrass even in favorable locations in the bay. Restoration plots near the mouth only survived when established during the spring (March) and slowly decline when established during the summer (July). This is the subject of ongoing research and will be reported elsewhere.

While this study was not intended to address the causes of the decline, other studies have shown that seagrass beds surviving under stressed conditions are more susceptible to events with rapid changes (e.g., storm events, dredging activities, etc.) that can lead to cascading negative effects and eventual loss of seagrasses (Moore, 2004). Self-amplifying feedbacks (both physical and biological) are a common feature in seagrass systems (Van der Heide et al., 2007; Maxwell et al., 2017; Moksnes et al., 2018). The ability of an eelgrass bed to locally

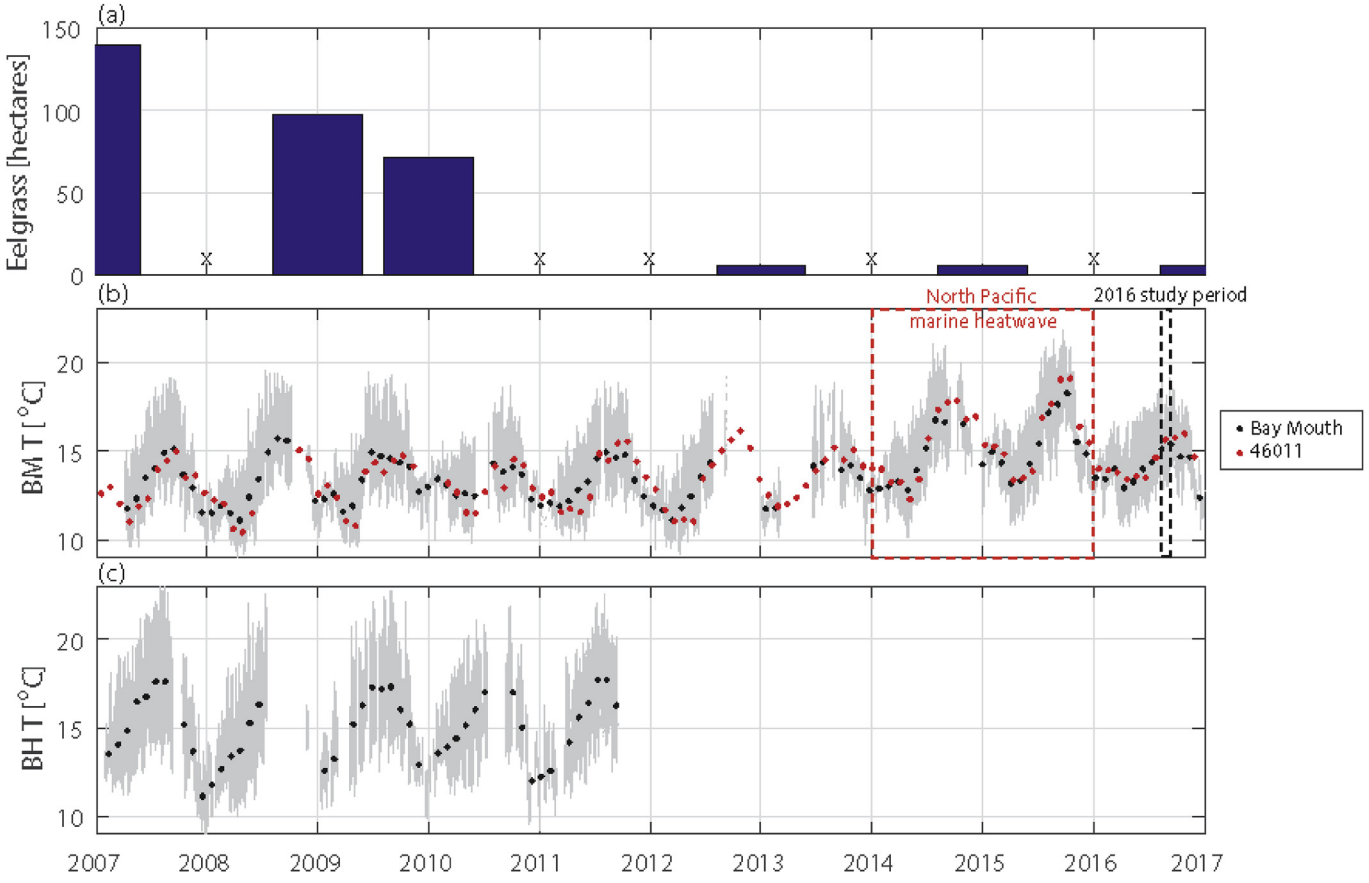

Fig. 10. Long-term records of (a) eelgrass coverage in Morro Bay, (b) temperature at the bay mouth (gray lines denote the 15 min data, black dots denote 30 day averages) and offshore (inner shelf) buoy 46011 (red dots denote 30 day averages), and (c) temperature at the bay head (gray lines denote the 15 min data, black dots denote 30 day averages). The red box in panel (b) delinieates the time period of the northeast Pacific marine heatwave, and the black box highlights the study period for the present study. (For interpretation of the references to color in this figure legend, the reader is referred to the Web version of this article.)

modify the physical and biological environment, where conditions are already marginal, likely aids in their success (Moore, 2004). However, when eelgrass starts to decline, the loss can cause further habitat and condition degradation that can lead to alternative states and local regime shifts that prevent recovery (Scheffer et al., 2001; Folke et al., 2004; Van der Heide et al., 2007; Carr et al., 2016; Maxwell et al., 2017; Moksnes et al., 2018). It is possible that the conditions in the back bay were marginal, and that some physical or biological change triggered the initial decline. Following self-amplifying feedbacks, the initial decline and subsequent transition from a vegetated to an unvegetated state, seems to have resulted in an alternative state in the back bay. If this is the case, the current distribution of eelgrass near the mouth may represent the extent of suitable environmental conditions locally in the bay for eelgrass populations.

In the case of Morro Bay, it is difficult to pinpoint the exact cause(s) of the decline given the lack of baseline monitoring prior to and during the decline, as is common in many unexpected ecosystem collapses. However, certain inferences can be made with the available data. Fig. 10 shows historical temperature measurements made at long-term monitoring stations at BM (2007–2017, Fig. 10b) and BH (2007–2011, Fig. 10c), as well as a surface buoy located on the shelf just offshore of Morro Bay (NDBC 46011, 2007–2017, Fig. 10b). Other quality-controlled historical water quality data were not available during this time period. Eelgrass started to decline from 2007 to 2010 (139–71 ha), and then between 2010 and 2013 eelgrass collapsed to 6 ha. Between 2007 and 2013, the seasonal temperature range and summer maximums in the bay did not change substantially, nor did the offshore shelf source waters (which are comparable to BM). Elevated temperatures associated with the northeast Pacific marine heatwave were not observed until after the collapse from 2014 to 2016 (i.e., the “warm blob” and El Niño, Gentemann et al., 2017). It therefore does not appear that abrupt changes in temperature led to the eelgrass collapse.

However, changes in sedimentation and bay geomorphology may have contributed to eelgrass collapse. Like many estuaries, Morro Bay has been heavily modified over the last century due to both climate and direct anthropogenic activities. Starting in the late 1800s, major land-use changes are reported to have increased the rate of sediment delivery to the bay (CCWQCB, 2002). In the early 1900s, one of the natural entrances to the bay was closed off. In the 1940s, the Army Corp of Engineers constructed breakwaters and a dike extending almost 500 m from Morro Rock to the adjacent land (CCWQCB, 2002), and they dredged the main channel to create navigation paths. Over the last century, it is estimated that the mean tidal prism in Morro Bay has decreased by over 20% with an average rate of sedimentation of 34,400 m^3 per year, although the watershed erosion and fluvial transport are noted to be extremely episodic based on regional climate (i.e., wet and dry years) (Haltiner and Thor, 1991). Moreover, the frequency of dredging increased from an average of once every five years between 1944 and 1975 to almost every year over the past several decades (CCWQCB, 2002, Fig. 2c). The salt marsh adjacent to Morro Bay has the highest observed sedimentation rates out of seven sites assessed in California and Mexico (Thorne et al., 2016). Similarly, a model with a constant and spatially uniform rate of long-term sedimentation predicted that Morro Bay will exhibit sediment-induced elevation changes, and subsequent loss of eelgrass habitat, over the next century, although the actual sedimentation in Morro Bay is likely to be more episodic both seasonally (i.e., during the wet winter season) and interannually (i.e., during wet years) (Shaughnessy et al., 2012).

It seems plausible that significant changes to the geomorphology of Morro Bay due to natural variability (e.g., climate, wet and dry years and the subsequent sediment loading) and direct and indirect anthropogenic causes (e.g., mouth modification, dredging, land-use practices) have resulted in changes in suitable bay habitat for eelgrass. Sedimentation and erosion greatly affect estuarine depth, and thus control eelgrass distributions by providing an upper and lower limit for survival. In a review of 45 case-studies worldwide, dredging was estimated to account for the loss of over 21,000 ha of seagrasses globally due to direct (e.g., physical removal) and indirect impacts (e.g., burial of eelgrass and effects of increased turbidity/decreased light due to suspended sediment) (Erftemeijer and Lewis, 2006). While eelgrass coverage has fluctuated naturally over time in Morro Bay, it never dropped below 39 ha and always rebounded within several years. Historical eelgrass coverage shows a large decline between 1994 and 1998, where eelgrass dropped to 39 ha, but later rebounded to near pre-decline levels by 2004. This particular event coincided with a wildfire in the adjacent watershed in August 1994, the largest dredging event on record starting in January 1995, and a series of high rainfall years reported to deposit substantial amounts of sediment into the bay (Fig. 2). During the most recent decline, a particularly wet year occurred in 2010 and coincided with a large dredging event in 2010 (Fig. 2). These events were followed by a series of dry years during an extended drought in California. It is possible that this series of events led to adverse conditions for eelgrass and contributed to the decline. Moreover, altered exchange processes and conditions in the bay may have led to significant regions that are no longer suitable for eelgrass survival (hence the failed restoration attempts). A project is currently underway to develop a high-resolution numerical sediment transport model to evaluate the link between eelgrass abundance and sediment processes by comparing historical and current eelgrass distributions to changes in modeled sediment dynamics to further test these ideas.

When considering dynamics and exchange processes in an estuary or embayment, as well as the ecological linkages, there is conventionally a match between length and time scales in that system (cf. Largier et al., 1997). That is, for small length-scale estuaries, residence and flushing times are also expected to be small. However, in LIEs during periods of hypersalinity, weak exchange between longitudinal zones can effectively decouple portions of the estuary, resulting in short systems with long residence and flushing times. The development of hypersalinity, both seasonally and over longer time periods, is sensitive to a host of natural and anthropogenic processes (see discussion in Largier et al., 1997), especially for shorter estuaries like Morro Bay (cf. Schettini et al., 2017). In particular, the longitudinal diffusivity and hydrodynamic exchange are strongly dependent on the geomorphology of the estuary. Thus, changes to bay geomorphology have the ability to significantly modify local environmental conditions. This research has important implications for assessing the role of climate and anthropogenic change in shaping nearshore ecosystems. LIEs are particularly sensitive to changes in climate (e.g., wet and dry years) and human disturbance (e.g., dredging and bay modification, land-use practices). Changes in hydrodynamics in a small estuary like Morro Bay potentially drive survival of species in both local- (aquatic) and global- (aviary, Pacific Flyway) scale ecosystems.

4. Conclusions

Morro Bay is a short, seasonally low-inflow estuary in central California that has recently experienced a rapid collapse of eelgrass, the major biogenic habitat in the bay. While large expanses of this foundational ecosystem were lost in the mid and back areas of the bay, the mouth still supports healthy and resilient beds. Using an array of oceanographic moorings throughout the bay, we observed that local environmental conditions in the back bay (where eelgrass has declined) were significantly different than those at the mouth (where eelgrass has persisted) during the summer, low-inflow season, with minimal hydrodynamic exchange between the two decoupled regions. Back-bay waters were warmer, more saline, less oxygenated, and more turbid, with longer flushing times, all of which have been shown to negatively affect eelgrass recovery and restoration. Regardless of what caused the initial eelgrass collapse, it appears that current conditions in the mid to back portions of the estuary are not conducive to eelgrass growth. The loss of eelgrass and ongoing lack of recovery in large portions of the estuary may be the result of both climate and direct anthropogenic influences on bay geomorphology, although further research is needed. In short estuaries like Morro Bay, small changes (both natural and anthropogenic) are amplified and habitat loss may occur more rapidly than longer estuaries. Ecosystems in LIEs may be especially prone to ecological regime shifts or collapse, and may require precautionary monitoring and management. Furthermore, for migratory animals, like brant geese, estuaries act as “stepping stones” along migratory routes. Loss of feeding grounds in a single estuary like Morro Bay may have profound consequences for the species on a much broader spatial scale. The Morro Bay system and the dramatic ecological change that it has experienced, demonstrate the critical role that hydrodynamics play in ecosystem health and habitat suitability, both locally and globally.

Acknowledgements

This publication was prepared by Walter and O'Leary under NOAA Grant #NA18OAR4170073, California Sea Grant College Program Project #R/HCE-07, through NOAA's National Sea Grant College Program, U.S. Department of Commerce. The statements, findings, conclusions and recommendations are those of the authors and do not necessarily reflect the views of California Sea Grant, NOAA or the U.S. Dept. of Commerce. This work was also supported by the Pacific States Marine Fisheries Commission (18-22G) . We also acknowledge support from the NOAA IOOS program through CeNCOOS for select oceanographic data collected at the Bay Mouth (BM) site and the meteorological data at the Bay Head (BH) site, including the long-term temperature measurements. Thermistors used at select sites were provided by the California Department of Fish and Wildlife. Finally, support was provided through Cal Poly's Research, Scholarly, and Creative Activities Grant Program. Boating resources and support were provided by the Cal Poly Center for Coastal Marine Sciences. We gratefully acknowledge help from staff at the Morro Bay National Estuary Program (MBNEP) including, but not limited to, Ann Kitajima, Carolyn Geraghty, and Karissa Willits. Aerial eelgrass data were obtained from the MBNEP. We also acknowledge support in the field from Ian Robbins, Grant Waltz, Brian Paavo, Jason Felton, Tom Moylan, and Brandon Shearer. Helpful conversations with Nicholas Nidzieko and Sean Vitousek are also acknowledged. Digital elevation model data for this region were obtained from NOAA's National Geophysical Data Center (Port San Luis region). Comments and suggestions from three anonymous reviewers greatly improved the quality of the manuscript.

References

Andersen, T., Carstensen, J., Hernández-García, E., Duarte, C.M., 2009. Ecological thresholds and regime shifts: approaches to identification. Trends Ecol. Evol. 24 (1), 49–57. https://doi.org/10.1016/j.tree.2008.07.014.

Beardsley, et al., 1985. CODE-2: Moored Array and Large-scale Data Report. CODE Technical Report No. 38, WHOI Technical Report 85-35.

Beca-Carretero, P., Olesen, B., Marbà, N., Krause-Jensen, D., 2018. Response to Experimental Warming in Northern Eelgrass Populations: Comparison across a Range of Temperature Conditions, vol 589. pp. 59–72. https://doi.org/10.3354/meps12439.

Burchard, H., 2011. Drivers of residual estuarine circulation in tidally energetic estuaries: straight and irrotational channels with parabolic cross section. J. Phys. Oceanogr. 41, 548–570. https://doi.org/10.1175/2010JPO4453.1.

Boch, C.A., Micheli, F., Alnajjar, M., Monismith, S.G., Beers, J.M., Bonilla, J.C., Espinoza, a. M., Vazquez-Vera, L., Woodson, C.B., 2018. Local oceanographic variability influences the performance of juvenile abalone under climate change. Sci. Rep. 8 (1), 1–12. https://doi.org/10.1038/s41598-018-23746-z.

Buck, C.M., Wilkerson, F.P., Parker, A.E., Dugdale, R.C., 2014. The influence of coastal nutrients on phytoplankton productivity in a shallow low inflow estuary, drakes

estero, California (USA). Estuar. Coast 37, 847–863. https://doi.org/10.1007/s12237-013-9737-6.
Bulthuis, D.A., 1987. Effects of temperature on photosynthesis and growth of seagrasses. Aquat. Bot. 27 (1), 27–40. https://doi.org/10.1016/0304-3770(87)90084-2.
Carr, J.A., D'Odorico, P., McGlathery, K.J., Wiberg, P.L., 2016. Spatially explicit feedbacks between seagrass meadow structure, sediment and light: habitat suitability for seagrass growth. Adv. Water Resour. 93, 315–325. https://doi.org/10.1016/j.advwatres.2015.09.001.
Central Coast Water Quality Control Board, 2002. Morro Bay total Maximum Daily Load for Sediment (Including Chorro Creek, Los Osos Creek and the Morro Bay Estuary). retrieved from. https://www.waterboards.ca.gov/rwqcb3/board_decisions/adopted_orders/2002/2002_0051_mb_sed_tmdl_final_proj_rpt.pdf July 2018.
Collier, C.J., Waycott, M., 2014. Temperature extremes reduce seagrass growth and induce mortality. Mar. Pollut. Bull. 83 (2), 483–490. https://doi.org/10.1016/j.marpolbul.2014.03.050.
Cheng, R.T., Ling, C., Gartner, J.W., 1999. Estimates of bottom roughness length and bottom shear stress in South San Francisco Bay, California. J. Geophys. Res. Ocean. 104 (C4), 7715–7728. https://doi.org/10.1029/1998JC900126.
Chou, Y., Nelson, K.S., Holleman, R.C., Fringer, O.B., Stacey, M.T., Lacy, J.R., Monismith, S.G., Koseff, J.R., 2018. Three-dimensional modeling of fine sediment transport by waves and currents in a shallow estuary. J. Geophys. Res. Ocean. https://doi.org/10.1029/2017JC013064.
Erftemeijer, P.L.A., Lewis III, R. R. Robin, 2006. Environmental impacts of dredging on seagrasses: a review. Mar. Pollut. Bull. 52 (12). https://doi.org/10.1016/j.marpolbul.2006.09.006.
Folke, C., Carpenter, S., Walker, B., Scheffer, M., Elmqvist, T., Gunderson, L., Holling, C.S., 2004. Regime shifts, resilience, and biodiversity in ecosystem management. Annu. Rev. Ecol. Evol. Syst. 35, 557–581. https://doi.org/10.1146/annurev.ecolsys.35.021103.105711.
Fonseca, M.S., Uhrin, A., 2009. The status of eelgrass , zostera marina, as bay scallop habitat: consequences for the fishery in the western atlantic. US Natl. Mar. Fish. Serv. Mar. Fish. Rev. 71, 20–33.
Gentemann, C.L., Fewings, M.R., García-Reyes, M., 2017. Satellite sea surface temperatures along the West Coast of the United States during the 2014-2016 northeast Pacific marine heat wave. Geophys. Res. Lett. 44, 312–319. https://doi.org/10.1002/2016GL071039.
Greve, T.M., Borum, J., Pedersen, O., 2003. Meristematic oxygen variability in eelgrass (Zostera marina). Limnol. Oceanogr. 48 (1), 210–216. https://doi.org/10.4319/lo.2003.48.1.0210.
Gross, T.F., Nowell, A.R.M., 1983. Mean flow and turbulence scaling in a tidal boundary layer. Continent. Shelf Res. 2 (2), 109–126. https://doi.org/10.1016/0278-4343(83)90011-0.
Halpern, B.S., et al., 2008. A global map of human impact on marine ecosystems. Science 319 (5865), 948–952.
Haltiner, J.P., Thor, D., 1991. Sedimentation processes in Morro bay, California. In: Proceedings: Coastal Sediments Conference, ASCE Waterway, Ports, Coastal, and Ocean Division, Seattle, WA, June 1991.
Hansen, J.C., Reidenbach, M.A., 2013. Seasonal growth and senescence of a zostera marina seagrass meadow alters wave-dominated flow and sediment suspension within a coastal bay. Estuar. Coast 36 (6), 1099–1114. https://doi.org/10.1007/s12237-013-9620-5.
Hansen, J.C., Reidenbach, M.A., 2012. Wave and tidally driven flows in eelgrass beds and their effect on sediment suspension. Mar. Ecol. Prog. Ser. 448, 271–287. https://doi.org/10.3354/meps09225.
Holsman, K.K., McDonald, P.S., Armstrong, D.A., 2006. Intertidal migration and habitat use by subadult Dungeness crab Cancer magister in a NE Pacific estuary. Mar. Ecol. Prog. Ser. 308, 183–195. https://doi.org/10.3354/meps308183.
Kaldy, J.E., 2014. Effect of temperature and nutrient manipulations on eelgrass Zostera marina L. from the Pacific Northwest, USA. J. Exp. Mar. Biol. Ecol. 453, 108–115. https://doi.org/10.1016/j.jembe.2013.12.020.
Lacy, J.R., Wyllie-Echeverria, S., 2011. The influence of current speed and vegetation density on flow structure in two macrotidal eelgrass canopies. Limnol. Oceanogr. Fluid. Environ. 1, 38–55. https://doi.org/10.1215/21573698-1152489.
Largier, J., 2010. Low-inflow estuaries: hypersaline, inverse, and thermal scenarios. In: Valle-Levinson, A. (Ed.), Contemporary Issues in Estuarine Physics. Cambridge University Press, Cambridge, pp. 247–272.
Largier, J.L., Hearn, C.J., Chadwick, D.B., 2013. Density structures in “low inflow estuaries. Buoyancy Eff. Coast. Estuar. Dyn. https://doi.org/10.1029/CE053p0227.
Largier, J.L., Hollibaugh, J.T., Smith, S.V., 1997. Seasonally hypersaline estuaries in Mediterranean-climate regions. Estuar. Coast Shelf Sci. 45 (6), 789–797. https://doi.org/10.1006/ecss.1997.0279.
Li, C., O'Donnell, J., 2005. The effect of channel length on the residual circulation in tidally dominated channels. J. Phys. Oceanogr. 35, 1826–1840. https://doi.org/10.1175/JPO2804.1.
Mayer, A.L., Rietkerk, M., 2004. The dynamic regime concept for ecosystem management and restoration. Bioscience 54 (11), 1013–1020. https://doi.org/10.1641/0006-3568(2004)054[1013:TDRCFE]2.0.CO;2.
Maxwell, P.S., et al., 2017. The fundamental role of ecological feedback mechanisms for the adaptive management of seagrass ecosystems – a review. Biol. Rev. 92 (3), 1521–1538. https://doi.org/10.1111/brv.12294.
Moksnes, P.O., Eriander, L., Infantes, E., Holmer, M., 2018. Local regime shifts prevent natural recovery and restoration of lost eelgrass beds along the Swedish West Coast. Estuar. Coast 1–20. https://doi.org/10.1007/s12237-018-0382-y.
Monismith, S.G., Kimmerer, W., Burau, J.R., Stacey, M.T., 2002. Structure and flow-induced variability of the subtidal salinity field in northern san Francisco bay. J. Phys. Oceanogr. 32 (11), 3003–3019. https://doi.org/10.1175/1520-0485(2002)032<3003:SAFIVO>2.0.CO;2.
Monismith, S.G., Jones, N., Bela, M., Nidzieko, N.J., Paytan, A., Misra, G., Street, J., 2005. Hydrodynamics and Sediment Dynamics in Elkhorn Slough. A report to Monterey Bay Sanctuary Foundation, December 2005, 1–83.
Morgan, S.G., Fisher, J.L., McAfee, S.T., Largier, J.L., Miller, S.H., Sheridan, M.M., Neigel, J.E., 2014. Transport of Crustacean larvae between a low-inflow estuary and coastal waters. Estuar. Coast 37, 1269–1283. https://doi.org/10.1007/s12237-014-9772-y.
Moore, K.A., 2004. Influence of seagrasses on water quality in shallow regions of the lower chesapeake bay. J. Coast Res. 10045, 162–178. https://doi.org/10.2112/SI45-162.1.
Moore, K.A., Shields, E.C., Parrish, D.B., 2014. Impacts of varying estuarine temperature and light conditions on *Zostera marina* (eelgrass) and its interactions with *Ruppia maritima* (widgeongrass). Estuar. Coast 37. https://doi.org/10.1007/s12237-013-9667-3.
Moore, K.A., Shields, E.C., Parrish, D.B., Orth, R.J., 2012. Eelgrass survival in two contrasting systems: role of turbidity and summer water temperatures. Mar. Ecol. Prog. Ser. 448, 247–258. https://doi.org/10.3354/meps09578.
Moore, K.A., Wetzel, R.L., Orth, R.J., 1997. Seasonal pulses of turbidity and their relations to eelgrass (Zostera marina L.) survival in an estuary. J. Exp. Mar. Biol. Ecol. 215 (1), 115–134. https://doi.org/10.1016/S0022-0981(96)02774-8.
Moore, K.A., Neckles, H., Orth, R., 1996. Zostera marina (eelgrass) growth and survival along a gradient of nutrients and turbidity in the lower Chesapeake Bay. Mar. Ecol. Prog. Ser. 142, 247–259. https://doi.org/10.3354/meps142247. February 2016.
Morro Bay National Estuary Program, 2013. Morro Bay Eelgrass Report 2013. retrieved from. http://www.mbnep.org/wp-content/uploads/2018/01/2013-Eelgrass-Monitoring-Report.pdf, Accessed date: May 2018.
Morro Bay National Estuary Program, 2015. Sediment Monitoring Report 2015. retrieved from. http://www.mbnep.org/wp-content/uploads/2014/12/2015-Sediment-Report.pdf, Accessed date: July 2018.
Morro Bay National Estuary Program, 2017. Morro Bay Eelgrass Report 2014 to 2016. retrieved from. http://www.mbnep.org/wp-content/uploads/2014/12/2014-2016-Eelgrass-Report.pdf, Accessed date: May 2018.
Nidzieko, N.J., 2010. Tidal asymmetry in estuaries with mixed semidiurnal/diurnal tides. J. Geophys. Res. Ocean. 115 (C8). https://doi.org/10.1029/2009JC005864.
Nidzieko, N.J., Ralston, D.K., 2012. Tidal asymmetry and velocity skew over tidal flats and shallow channels within a macrotidal river delta. J. Geophys. Res. Ocean. 117 (C3). https://doi.org/10.1029/2011JC007384.
Nidzieko, N.J., Monismith, S.G., 2013. Contrasting seasonal and fortnightly variations in the circulation of a seasonally inverse estuary, elkhorn slough, California. Estuar. Coast 36 (1), 1–17. https://doi.org/10.1007/s12237-012-9548-1.
Nyström, M., Norström, A.V., Blenckner, T., de la Torre-Castro, M., Eklöf, J.S., Folke, C., Österblom, H., Steneck, R.S., Thyresson, M., Troell, M., 2012. Confronting feedbacks of degraded marine ecosystems. Ecosystems 15 (5), 695–710. https://doi.org/10.1007/s10021-012-9530-6.
Orth, R.J., Carruthers, T.J.B., Dennison, W.C., Duarte, C.M., Fourqurean, J.W., Heck, K.L., Hughes, A.R., Kendrick, G.A., Kenworthy, W.J., Olyarnik, S., Short, F.T., Waycott, M., Williams, S.L., 2006. A global crisis for seagrass ecosystems. Bioscience 56 (12), 987–996. https://doi.org/10.1641/0006-3568(2006)56[987:AGCFSE]2.0.CO;2.
Phelan, P.J., Steinbeck, J., Walter, R.K., 2018. Influence of internal bores on larval fish abundance and community composition. Reg. Stud. Mar. Sci. 20, 1–12. https://doi.org/10.1016/j.rsma.2018.03.010.
Reidenbach, M.A., Monismith, S.G., Koseff, J.R., 2006. Boundary layer turbulence and flow structure over a fringing coral reef. 51 (5), 1956–1968.
Rosenfeld, L.K., Schwing, F.B., Garfield, N., Tracy, D.E., 1994. Bifurcated flow from an upwelling center: a cold water source for Monterey Bay. Continent. Shelf Res. 14 (9), 931–964.
Scheffer, M., Carpenter, S., Foley, J.A., Folke, C., Walker, B., 2001. Catastrophic shifts in ecosystems. Nature 413 (6856), 591–596. https://doi.org/10.1038/35098000.
Schettini, C.A.F., Valle-Levinson, A., Truccolo, E.C., 2017. Circulation and transport in short, low-inflow estuaries under anthropogenic stresses. Reg. Stud. Mar. Sci. 10, 52–64. https://doi.org/10.1016/j.rsma.2017.01.004.
Shaughnessy, F.J., Gilkerson, W., Black, J.M., Ward, D.H., Petrie, M., 2012. Predicted eelgrass response to sea level rise and its availability to foraging Black Brant in Pacific coast estuaries. Ecol. Appl. 22 (6), 1743–1761. https://doi.org/10.1890/11-1083.1.
Short, F.T., Wyllie-Echeverria, S., 1996. Natural and human-induced disturbance of seagrasses. Environ. Conserv. 23 (1), 17. https://doi.org/10.1017/S0376892900038212.
Suanda, S.H., Barth, J.A., Woodson, C.B., 2011. Diurnal heat balance for the northern Monterey Bay inner shelf. J. Geophys. Res. Ocean. 116 (9). https://doi.org/10.1029/2010JC006894.
Tetra Tech, Inc, 1999. Morro Bay National Estuary Program Hydrodynamic Circulation Model, Lafayette, CA.
Thorne, K., et al., 2016. Effects of Climate Change on Tidal Marshes along a Latitudinal Gradient in California. pp. 75. https://doi.org/10.3133/ofr20161125. United State Geological Survey Open-File Report 2016-1125.
Van der Heide, T., Van Nes, E.H., Geerling, G.W., Smolders, A.J.P., Bouma, T.J., Van Katwijk, M.M., 2007. Positive feedbacks in seagrass ecosystems: implications for success in conservation and restoration. Ecosystems 10 (8), 1311–1322. https://doi.org/10.1007/s10021-007-9099-7.
Vaquer-Sunyer, R., Duarte, C.M., 2008. Thresholds of hypoxia for marine biodiversity. Proc. Natl. Acad. Sci. Unit. States Am. 105 (40), 15452–15457. https://doi.org/10.1073/pnas.0803833105.
Walter, R.K., Armenta, K.J., Shearer, B., Robbins, I., Steinbeck, J., 2018. Coastal upwelling seasonality and variability of temperature and chlorophyll in a small coastal embayment. Continent. Shelf Res. 154. https://doi.org/10.1016/j.csr.2018.01.002.
Walter, R.K., Reid, E.C., Davis, K.A., Armenta, K.J., Merhoff, K., Nidzieko, N.J., 2017.

Local diurnal wind-driven variability and upwelling in a small coastal embayment. J. Geophys. Res. Ocean. 122 (2), 955–972. https://doi.org/10.1002/2016JC012466.
Walter, R.K., Nidzieko, N.J., Monismith, S.G., 2011. Similarity scaling of turbulence spectra and cospectra in a shallow tidal flow. J. Geophys. Res. Ocean. 116 (10), 1–14. https://doi.org/10.1029/2011JC007144.
Waycott, M., et al., 2009. Accelerating loss of seagrasses across the globe threatens coastal ecosystems. Proc. Natl. Acad. Sci. Unit. States Am. 106 (30), 12377–12381. https://doi.org/10.1073/pnas.0905620106.
Wilson, M.L., Webster, D.R., Weissburg, M.J., 2013. Spatial and temporal variation in the hydrodynamic landscape in intertidal salt marsh systems. Limnol. Oceanogr. Fluid. Environ. 3 (0), 156–172. https://doi.org/10.1215/21573689-2373360.
Zimmerman, R.C., Steller, D.L., Kohrs, D.G., Alberte, R.S., 2001. Top-down impact through a bottom-up mechanism. In situ effects of limpet grazing on growth, light requirements and survival of the eelgrass Zostera marina. Mar. Ecol. Prog. Ser. 218, 127–140. https://doi.org/10.3354/meps218127.